Biomedical Optics EXPRESS

In vivo quantitation of injected circulating tumor cells from great saphenous vein based on video-rate confocal microscopy

Howon Seo, Yoonha Hwang, Kibaek Choe, and Pilhan Kim*

Graduate School of Nanoscience and Technology, Korea Advanced Institute of Science and Technology (KAIST), Daehak-ro 291, Yuseong-gu, Daejeon, 305-701, South Korea
*pilhan.kim@kaist.ac.kr

Abstract: The number of circulating tumor cell (CTC) in the peripheral blood of cancer patients can be a valuable biomarker for cancer diagnosis and treatment monitoring. In this study, we implemented a custom-design video-rate confocal microscopy system in capable of direct visualization of fast flowing CTC at great saphenous vein (GSV) of a live animal model *in vivo*. Continuous acquisition of video-rate images at GSV revealed the highly dynamic time-dependent changes in the number of intravenously injected circulating tumor cells. By extracting a calibration factor through the hemocytometric analysis of intravenously injected long-circulating red blood cells, we established a novel quantitation method for CTC in whole body blood *in vivo*.

©2015 Optical Society of America

OCIS codes: (170.1470) Blood or tissue constituent monitoring; (170.1790) Confocal microscopy; (170.2520) Fluorescence microscopy; (000.1430) Biology and medicine.

References and links

1. S. Valastyan and R. A. Weinberg, "Tumor metastasis: molecular insights and evolving paradigms," Cell **147**(2), 275–292 (2011).
2. G. P. Gupta and J. Massagué, "Cancer metastasis: building a framework," Cell **127**(4), 679–695 (2006).
3. P. S. Steeg, "Tumor metastasis: mechanistic insights and clinical challenges," Nat. Med. **12**(8), 895–904 (2006).
4. A. F. Chambers, A. C. Groom, and I. C. MacDonald, "Dissemination and growth of cancer cells in metastatic sites," Nat. Rev. Cancer **2**(8), 563–572 (2002).
5. J. A. Joyce and J. W. Pollard, "Microenvironmental regulation of metastasis," Nat. Rev. Cancer **9**(4), 239–252 (2009).
6. H. Ledford, "Cancer theory faces doubts," Nature **472**(7343), 273 (2011).
7. I. J. Fidler, "Metastasis: quantitative analysis of distribution and fate of tumor embolilabeled with 125 I-5-Iodo-2′-Deoxyuridine," J. Natl. Cancer Inst. **45**(4), 773–782 (1970).
8. S. J. Cohen, C. J. Punt, N. Iannotti, B. H. Saidman, K. D. Sabbath, N. Y. Gabrail, J. Picus, M. Morse, E. Mitchell, M. C. Miller, G. V. Doyle, H. Tissing, L. W. Terstappen, and N. J. Meropol, "Relationship of circulating tumor cells to tumor response, progression-free survival, and overall survival in patients with metastatic colorectal cancer," J. Clin. Oncol. **26**(19), 3213–3221 (2008).
9. M. Cristofanilli, L. W. M. M. Terstappen, and D. F. Hayes, "Circulating epithelial cells in breast cancer - Reply," N. Engl. J. Med. **351**, 2453–2454 (2004).
10. M. C. Miller, G. V. Doyle, and L. W. Terstappen, "Significance of circulating tumor cells detected by the CellSearch system in patients with metastatic breast colorectal and prostate cancer," J. Oncol. **2010**, 617421 (2010).
11. M. Yu, S. Stott, M. Toner, S. Maheswaran, and D. A. Haber, "Circulating tumor cells: approaches to isolation and characterization," J. Cell Biol. **192**(3), 373–382 (2011).
12. S. Nagrath, L. V. Sequist, S. Maheswaran, D. W. Bell, D. Irimia, L. Ulkus, M. R. Smith, E. L. Kwak, S. Digumarthy, A. Muzikansky, P. Ryan, U. J. Balis, R. G. Tompkins, D. A. Haber, and M. Toner, "Isolation of rare circulating tumour cells in cancer patients by microchip technology," Nature **450**(7173), 1235–1239 (2007).
13. S. L. Stott, C. H. Hsu, D. I. Tsukrov, M. Yu, D. T. Miyamoto, B. A. Waltman, S. M. Rothenberg, A. M. Shah, M. E. Smas, G. K. Korir, F. P. Floyd, Jr., A. J. Gilman, J. B. Lord, D. Winokur, S. Springer, D. Irimia, S. Nagrath, L. V. Sequist, R. J. Lee, K. J. Isselbacher, S. Maheswaran, D. A. Haber, and M. Toner, "Isolation of circulating tumor cells using a microvortex-generating herringbone-chip," Proc. Natl. Acad. Sci. U.S.A. **107**(43), 18392–18397 (2010).
14. H. Lee, E. Sun, D. Ham, and R. Weissleder, "Chip-NMR biosensor for detection and molecular analysis of cells," Nat. Med. **14**(8), 869–874 (2008).
15. C. Alix-Panabières, H. Schwarzenbach, and K. Pantel, "Circulating tumor cells and circulating tumor DNA," Annu. Rev. Med. **63**(1), 199–215 (2012).

#235885 - $15.00 USD Received 9 Mar 2015; revised 8 May 2015; accepted 14 May 2015; published 19 May 2015

16. R. A. Ghossein, S. Bhattacharya, and J. Rosai, "Molecular detection of micrometastases and circulating tumor cells in solid tumors," Clin. Cancer Res. **5**(8), 1950–1960 (1999).
17. X. Zhe, M. L. Cher, and R. D. Bonfil, "Circulating tumor cells: finding the needle in the haystack," Am. J. Cancer Res. **1**(6), 740–751 (2011).
18. Z. C. Fan, J. Yan, G. D. Liu, X. Y. Tan, X. F. Weng, W. Z. Wu, J. Zhou, and X. B. Wei, "Real-time monitoring of rare circulating hepatocellular carcinoma cells in an orthotopic model by in vivo flow cytometry assesses resection on metastasis," Cancer Res. **72**(10), 2683–2691 (2012).
19. I. Georgakoudi, N. Solban, J. Novak, W. L. Rice, X. Wei, T. Hasan, and C. P. Lin, "In vivo flow cytometry: A new method for enumerating circulating cancer cells," Cancer Res. **64**(15), 5044–5047 (2004).
20. W. He, H. Wang, L. C. Hartmann, J. X. Cheng, and P. S. Low, "In vivo quantitation of rare circulating tumor cells by multiphoton intravital flow cytometry," Proc. Natl. Acad. Sci. U.S.A. **104**(28), 11760–11765 (2007).
21. J. Novak, I. Georgakoudi, X. Wei, A. Prossin, and C. P. Lin, "In vivo flow cytometer for real-time detection and quantification of circulating cells," Opt. Lett. **29**(1), 77–79 (2004).
22. Y. Ding, J. Wang, Z. Fan, D. Wei, R. Shi, Q. Luo, D. Zhu, and X. Wei, "Signal and depth enhancement for in vivo flow cytometer measurement of ear skin by optical clearing agents," Biomed. Opt. Express **4**(11), 2518–2526 (2013).
23. Y. A. Menyaev, D. A. Nedosekin, M. Sarimollaoglu, M. A. Juratli, E. I. Galanzha, V. V. Tuchin, and V. P. Zharov, "Optical clearing in photoacoustic flow cytometry," Biomed. Opt. Express **4**(12), 3030–3041 (2013).
24. M. Sarimollaoglu, D. A. Nedosekin, Y. Simanovsky, E. I. Galanzha, and V. P. Zharov, "In vivo photoacoustic time-of-flight velocity measurement of single cells and nanoparticles," Opt. Lett. **36**(20), 4086–4088 (2011).
25. E. I. Galanzha, E. V. Shashkov, P. M. Spring, J. Y. Suen, and V. P. Zharov, "In vivo, noninvasive, label-free detection and eradication of circulating metastatic melanoma cells using two-color photoacoustic flow cytometry with a diode laser," Cancer Res. **69**(20), 7926–7934 (2009).
26. E. I. Galanzha and V. P. Zharov, "Photoacoustic flow cytometry," Methods **57**(3), 280–296 (2012).
27. K. Polyak and R. A. Weinberg, "Transitions between epithelial and mesenchymal states: acquisition of malignant and stem cell traits," Nat. Rev. Cancer **9**(4), 265–273 (2009).
28. M. Yu, D. T. Ting, S. L. Stott, B. S. Wittner, F. Ozsolak, S. Paul, J. C. Ciciliano, M. E. Smas, D. Winokur, A. J. Gilman, M. J. Ulman, K. Xega, G. Contino, B. Alagesan, B. W. Brannigan, P. M. Milos, D. P. Ryan, L. V. Sequist, N. Bardeesy, S. Ramaswamy, M. Toner, S. Maheswaran, and D. A. Haber, "RNA sequencing of pancreatic circulating tumour cells implicates WNT signalling in metastasis," Nature **487**(7408), 510–513 (2012).
29. J. H. Taube, J. I. Herschkowitz, K. Komurov, A. Y. Zhou, S. Gupta, J. Yang, K. Hartwell, T. T. Onder, P. B. Gupta, K. W. Evans, B. G. Hollier, P. T. Ram, E. S. Lander, J. M. Rosen, R. A. Weinberg, and S. A. Mani, "Core epithelial-to-mesenchymal transition interactome gene-expression signature is associated with claudin-low and metaplastic breast cancer subtypes," Proc. Natl. Acad. Sci. USA **107**(35), 15449–15454 (2010).
30. N. Aceto, A. Bardia, D. T. Miyamoto, M. C. Donaldson, B. S. Wittner, J. A. Spencer, M. Yu, A. Pely, A. Engstrom, H. Zhu, B. W. Brannigan, R. Kapur, S. L. Stott, T. Shioda, S. Ramaswamy, D. T. Ting, C. P. Lin, M. Toner, D. A. Haber, and S. Maheswaran, "Circulating tumor cell clusters are oligoclonal precursors of breast cancer metastasis," Cell **158**(5), 1110–1122 (2014).
31. M. Yu, A. Bardia, B. S. Wittner, S. L. Stott, M. E. Smas, D. T. Ting, S. J. Isakoff, J. C. Ciciliano, M. N. Wells, A. M. Shah, K. F. Concannon, M. C. Donaldson, L. V. Sequist, E. Brachtel, D. Sgroi, J. Baselga, S. Ramaswamy, M. Toner, D. A. Haber, and S. Maheswaran, "Circulating breast tumor cells exhibit dynamic changes in epithelial and mesenchymal composition," Science **339**(6119), 580–584 (2013).
32. K. Choe, Y. Hwang, H. Seo, and P. Kim, "In vivo high spatiotemporal resolution visualization of circulating T lymphocytes in high endothelial venules of lymph nodes," J. Biomed. Opt. **18**(3), 036005 (2013).
33. Y. Hwang, J. Ahn, J. Mun, S. Bae, Y. U. Jeong, N. A. Vinokurov, and P. Kim, "In vivo analysis of THz wave irradiation induced acute inflammatory response in skin by laser-scanning confocal microscopy," Opt. Express **22**(10), 11465–11475 (2014).

1. Introduction

Circulating tumor cell (CTC) refers a cancer cell that have entered bloodstream from the primary tumor and survived in the blood circulation, which can extravasate to a distant organ and form new tumor colony [1]. This spread of tumor cells from the primary tumor to distant organs, called as a metastasis, is the major cause of cancer-related deaths from solid tumors (~90%) by causing vital organ failure [2, 3]. Cancer metastasis is a highly complicated process consists of multiple steps: the primary tumor growth, cancer cell mobilization and invasion into surrounding tissue, intravasation into a blood vessel, circulation in the blood stream, extravasation to distant site, and the formation of new tumor [1, 4–6]. Throughout these complex progressive steps, the survival during the circulation in the blood stream is considered as the most critical checkpoint for cancer cell to spread to distant organs. Although a number of cancer cells can routinely intravasate into the blood circulation, it have been suggested that much less than one of ten thousands

of CTC can survive to form distant metastasis [4, 7]. There has been an increasing number of studies reporting the correlation between the number of CTC and the risk of cancer metastasis, showing that an increased number of CTC in the peripheral blood sample is significantly related with shorter progression-free and overall survival in patients with metastatic breast, lung, colorectal and prostate [8–10]. Therefore, the quantitation of CTCs in the blood of metastatic cancer patients can provide valuable information for the precise monitoring of cancer metastasis, the evaluation of response to anti-cancer treatment and the early detection of cancer recurrence.

In the past decade, several techniques for the detection of CTCs from peripheral blood samples have been developed, including the CellSearch system (Veridex) approved by FDA [9, 11], microfluidics platform [12, 13], chip-based diagnostic MRI (DMR) biosensor [14] and real-time PCR [15]. However, those *ex vivo* techniques using a peripheral blood sample drawn from the patient have been suffered low success rate of CTC detection. It is principally due to two combined limiting factors. One is the limited volume of blood allowed to draw from the patient (about 10 milliliter per each draw) and the other is the extreme rarity of CTC in blood (less than one CTC per one milliliter of blood [16, 17]). These factors make only a handful number of CTCs present in the blood sample of most cancer patients to begin with, which is the principal barrier in establishing *ex vivo* CTC detection techniques as a common tool in cancer treatment. To note, these limiting factors could much more adversely limit the detection of CTC from the blood sample of patients in the relatively early stages of cancer such as stage 2B and 3 or patients in partial remission for whom a close monitoring of cancer progression and the efficacy of anti-cancer treatment, potentially using CTC as a surrogate marker, may provide the most profound clinical benefit.

In vivo flow cytometry (IVFC) capable of direct detection of circulating tumor cell from the blood vessels in a living animal [18–21] can be one of approaches to overcome these barriers. Given enough time, IVFC can analyze much larger volume of bloods than *ex vivo* detection techniques, because it is not limited to the small volume of *ex vivo* blood sample but analyzing continuous flow of blood inside a blood vessel *in vivo* [22–24]. However, most of previous reports have focused on small capillary vessel with diameter of several tens of micrometer in which the blood flow is quite slow (100-200 μm/sec); thus the analyzed blood volume analyzed for a given time was minimal. It was partly due to the slow image acquisition speed of common laser-scanning microscopy system and the consequent difficulty in the detection and quantitation of rapidly flowing cells in larger blood vessel in which the blood flow is much faster (>2mm/sec). To note, a photoacoustic detection of CTCs have been performed on large vessels (e.g. 0.9 mm aorta) with fast flow [25, 26], though it didn't capture the images of flowing CTCs *in situ*. Nevertheless, most of *in vivo* flow cytometry studies have detected flowing CTCs as a sudden spike in the continuously detected signal. However it only provides the information about the number of fluorescent objects passing through the focal volume of external light inside the vessel, which lack the morphological information such as cell size and subcellular features, as well as dynamic information about the CTC behavior in blood. More importantly, recent studies have reported the dynamic formation of CTC cluster in blood [27–29] and its implication to increased risk of metastasis [30, 31]. Collectively, a direct imaging method to capture the microscopic images of flowing CTCs and their cluster, preferentially in large vessel with fast blood flow to analyze more blood volume in a given time, and a quantitation method for the images to provide dynamic morphological information of CTCs have become highly desirable.

In this study, we implemented a custom-design video-rate confocal microscopy system based on fast-rotating polygonal mirror. The system could acquire sub-micron resolution images with the size of 512x512 pixels at video rate (30 frames per second). It allowed us a direct real-time imaging of rapidly flowing individual cells in the great saphenous vein (GSV) of which the diameter is typically about 500 μm. GSV circulates about three orders of magnitude more blood than the small capillary vessel, providing significantly increased amount of blood for IVFC analysis. To verify the capability of the implemented system for the direct imaging of CTC at GSV, we intravenously injected

#235885 - $15.00 USD Received 9 Mar 2015; revised 8 May 2015; accepted 14 May 2015; published 19 May 2015
(C) 2015 OSA

CT26 colorectal cancer cells labeled with green fluorescence dye, carboxyfluorescein succinimidyl ester (CFSE) and successfully acquired the clear image of flowing CT26 cells in the GSV. And we continuously acquired video-rate images of GSV, which revealed the highly dynamic time-dependent changes in the number of circulating CT26 cells. The number of flowing CT26 cell detected at GSV steadily increased right after the injection and reached the maximum at 1.5 minutes after the injection as it took some time to be evenly mixed with the systemically circulating blood in the body. Then, interestingly, it rapidly decreased to below the 10% of the maximum within 2 minutes due to the massive destruction of CT26 cells those were suddenly exposed to the harsh environment of blood circulation by the intravenous injection. At the same time we observed a large number of small-sized fluorescent particles those were presumably the cellular debris of CT26 cell destroyed in blood circulation. Indeed, the small debris was also quickly disappeared within 2 minutes along with the decrease of circulating CT26 cells. On the other hand, when we intravenously injected red blood cell (RBC) fluorescently labeled with far-red fluorophore - DiD, the number of flowing RBC detected at GSV increased and reached the maximum at 1.5 minutes like CT26 cell. Then, in contrast to the observation with the CT26 cell, the number of detected RBC was maintained at the initially reached maximum over 60 minutes, suggesting the long-term survival of RBC in blood circulation after the intravenous injection. This observation is fairly reasonable as RBC can naturally sustain harsh environment in blood circulation. Notably, from the pre-determined total number of injected RBCs stably maintained in blood circulation, we could calculate the relative calibration factor between the dynamically varying number of CT26 cells and estimate the total number of circulating CTC in whole body blood *in vivo*.

2. Experimental setup and methods

2.1 Video-rate intravital laser-scanning confocal microscope system

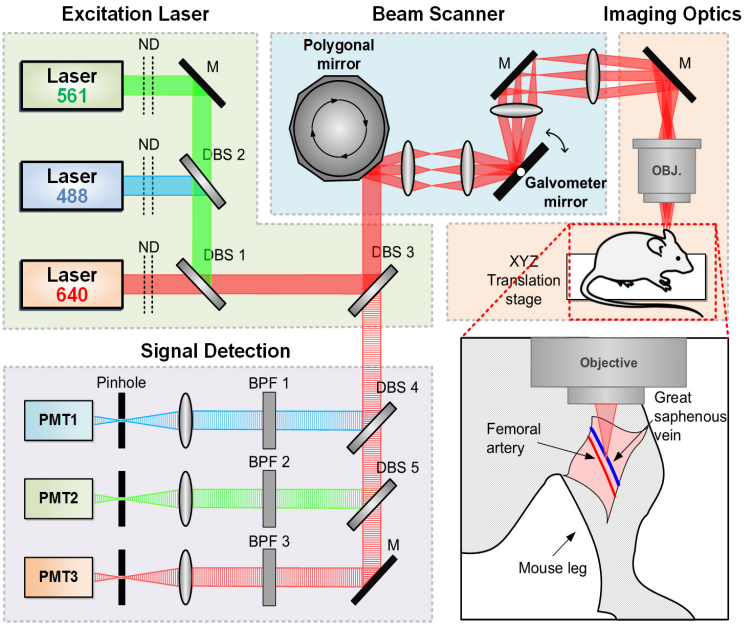

Fig. 1. Schematic of intravital custom-built video-rate laser scanning confocal microscope system and illustration of great saphenous vein (GSV) in the mouse leg: ND, neutral density filer; DBS, dichroic beam splitter; BPF, band pass filter; M, mirror; PMT, photomultiplier tube; OBJ, objective lens.

#235885 - $15.00 USD Received 9 Mar 2015; revised 8 May 2015; accepted 14 May 2015; published 19 May 2015
(C) 2015 OSA

Our intravital imaging platform was implemented by modifying the custom-built video-rate confocal laser-scanning microscope system previous developed [32, 33]. Figure 1 shows the schematics of the imaging system and illustration of great saphenous vein located in the mouse leg. Excitation laser beam paths were shown by solid lines and emitted fluorescence beam paths were shown by dashed lines. Three continuous-wave laser sources composed of 488nm diode laser module (MLD488, Cobolt), 561nm DPSS laser (Jive, Cobolt) and 640nm diode laser module (MLD640, Cobolt) were used as excitation light source. And intensity of each laser was independently adjusted by neutral density filter (Thorlabs, NDC-50C-4M-A). All three laser beams were combined by using dichroic beam splitters (DBS1; FF593-Di03, DBS2; FF520-Di02, Semrock) and then delivered to a multi-edge dichroic beam splitter (DBS3; Di01-R405/488/561/635, Semrock). The collinearly aligned laser beams were scanned by a fast rotating 36 facet polygonal mirror (MC-5, aluminum coated, Lincoln Laser) and a galvanometer mirror scanner (6230H, Cambridge Technology), generating a two-dimensional raster scanning pattern. The scanning laser beams were delivered to the great saphenous vein (GSV) of the anesthetized mouse on the XYZ translation stage (3DMS, Sutter Instrument) through a commercial long working-distance high N.A. objective lens (LUCPLFLN 40X, 0.60NA, Olympus), which provided the field of view of 250 × 250 μm. The three-color fluorescence signals from the sample were de-scanned and separated from the excitation laser beams by DBS3. Then, the signals were split into three individual fluorescence signals (green, red, and far-red) by the dichroic beam splitters (DBS4; FF560-Di01, DBS5; FF649-Di01, Semrock) and band pass filters (BPF1; FF01-525/45, BPF2; FF01-600/37, BPF3; FF01-697/58, Semrock). Confocal pinholes (#39-880, Edmund optics) were placed in front of each photomultiplier tube (PMT; R9110, Hamamatsu) used as fluorescence detectors. We used the pinhole much larger than the airy disk size (300 μm) to increase the z-sectioning thickness to have large detection volume. The z-sectioning thickness for detection is measured to be 8 μm. Electronic outputs from the PMTs were digitized using an 8-bit resolution 3-channel frame grabber (Solios, Matrox) with a sampling rate of 10 MHz for each channel. Triple-color images (512 × 512 pixels) were displayed and recorded in real time at video-rate of 30 Hz by custom-developed imaging software using Matrox Imaging Library (MIL9, Matrox).

2.2 Cells culture and fluorescent labelling

In this study, a CT26 murine colon carcinoma cell line was maintained in RPMI 1640 medium (Invitrogen) containing 10% fetal bovine serum (FBS; Invitrogen) and 1% penicillin-streptomycin (Invitrogen) and kept in a 5% CO2 incubator at 37°C. CT26 cells were harvested by trypsinization with 0.25% trypsin-EDTA (Invitrogen) and re-suspended in growth medium. Re-suspended CT26 cells were fluorescently labelled with Carboxy-fluorescein diacetate succinimidyl ester (CFSE; Invitrogen). Cell viability more than 95% after the labeling was confirmed by using the dead cell staining kit. Likewise CT26 cells, to visualize the fast flowing RBCs at GSV, 10μl of blood was drawn from the retro-orbital sinus of anesthetized mouse and fluorescently labelled with 1,1′-dioctadecyl-3,3,3′,3′-tetramethylin-dodicarbocyanine-perchlorate (DiD; Invitrogen). Labelled CT26 cells and RBCs were maintained at 4°C before intravenous injection into the lateral tail vein of anesthetized mice.

2.3 Animal imaging procedure

BALB/c mice aged 10~12 weeks were used. Mice were anesthetized by intramuscular injection of xylazine (10 mg/kg) and zoletile (30 mg/kg). The hair on the thigh was removed by hair clipper and hair removal cream. The GSV was surgically exposed by making a small skin incision and removing a subcutaneous fatty tissue. Tail vein catheter was used to inject fluorescent agents and cells. Tetramethyl-rhodamine (TAMRA) dextran conjugates (D-7139, Life Technology) were intravenously injected to label blood plasma, allowing the identification of GSV for imaging. Once the GSV is found, 3D translation stage is precisely manipulated to place the GSV at the center of the imaging field of view. The position of imaging focal plane in z-axis is adjusted to be located at 60

#235885 - $15.00 USD Received 9 Mar 2015; revised 8 May 2015; accepted 14 May 2015; published 19 May 2015
(C) 2015 OSA

μm inside the GSV wall. After starting a video-rate confocal movie recording, the fluorescent labelled CT26 cells and RBCs were intravenously injected through the tail vein catheter. The excitation laser power measured below the objective lens was 1 mW, 0.4 mW and 0.5 mW at 488 nm, 516 nm and 640 nm, respectively. During the imaging, the mouse body temperature was maintained at 37 °C by using a homeothermic control system (PhysioSuite, Kent Scientific). The temperature of the exposed tissue area surrounding GSV was also maintained at 37 °C with warm saline and additional heat pad. Animal care and all experiments were performed with the approval of the Animal Care Committee of KAIST (protocol no. KA2011-36).

2.4 Image processing

For the reliable quantitation of intact circulating cell, we devised an image processing algorithm to distinguish the small-sized particle and reasonable cell-sized object. Image processing was performed by using custom-written code of Matlab (Mathworks) after acquiring the real-time video-rate movie from the GSV. To analyze the time-dependent changes in the number of detected flowing cells in GSV, an AVI format video (30 frames/sec) was continuously recorded from right after the intravenous injection until 20 minutes. First, the video was converted into individual image sequence. All of the images were applied with 2D median filter of size 3 to eliminate isolated speckle noise and converted to binary image by thresholding of 50%. From each image, all of the connected components were automatically identified and their area in the unit of number of pixels was computed by using a Matlab function BWCONNCOMP in Image Processing Toolbox. As the pixel size is pre-characterized, we can determine the size of each component. After removing all of components smaller than the reasonable size of intact cell presumably cellular debris, the number of remaining components was counted as intact flowing cells. To exclude the possibility of counting a single cell appeared in consecutive frames multiple times, every consecutive frames those have identified cells were further analyzed. To note, the mouse leg was carefully positioned so that GSV wall and blood flow to be shown along the diagonal direction in the display. Within the imaging field of view of 250 μm, the most of flowing cells' trajectories are observed to be relatively parallel to GSV wall with ± 15° deviation. Therefore, for the identified cells appeared in consecutive frames, if the connecting trajectory between the positions of cells is deviated less than 15° deviated against the GSV wall, they were considered as a single cell appeared in multiple consecutive frames.

3. Results

3.1 In vivo imaging of intravenous injected circulating CT26 cells at GSV

We used a custom-built video-rate laser scanning confocal microscope system depicted in Fig. 1 for the direct imaging of circulating tumor cell (CTC) at GSV. GSV was selected as an imaging site because GSV is superficial vein at thigh that can be easily accessed by minimal surgery and GSV can be tightly fixed to minimize motion artifact. In addition, GSV is one of the largest veins in the whole body, which circulates about three orders of magnitude more blood than the small capillary vessel, providing large volume of blood for *in vivo* flow cytometry analysis. To verify the capability of the implemented system, we intravenously injected CT26 colorectal cancer cells labeled with green fluorescence dye, carboxyfluorescein succinimidyl ester (CFSE), to wildtype BALB/c mouse. The number of injected CT26 cell was 10^6. In addition, to visualize the blood plasma in GSV, 100μg of red fluorescent TAMRA-dextran was also intravenously injected. As shown in Fig. 2(a), we successfully acquired the clear image of flowing CT26 cells in the GSV. However, as it can be easily noticed, along with CT26 cells of which size is more than 7.5 μm, a large number of green fluorescent small objects were detected, which is mostly cell debris, not intact circulating CT26 cells. To exclude these small fragments from the CTC quantitation, we developed an image processing algorithm as described in section 2.4. It sequentially performs the identification of individual objects, calculation of its size, removal of objects smaller than a threshold, finally counting of objects in each image frames. Figure 2(a) shows the raw images and their image-processed results with various

#235885 - $15.00 USD Received 9 Mar 2015; revised 8 May 2015; accepted 14 May 2015; published 19 May 2015
(C) 2015 OSA

object size thresholds. Each row shows the outcomes with increasing the size threshold. Red circles mark the objects those were removed by increasing the size threshold. In this work, we used 7.5 μm as a size threshold to count intact CTCs.

Figure 2(b) shows the time-domain kinetics of circulating CT26 cells from the moment right after the intravenous injection for 20 minutes. Each symbol represents the number of detected CT26 cells for 30 seconds with different object size threshold. The detected number of circulating CT26 cell steadily increased after the IV injection and reached the maximum at 1.5 minutes. This suggests that it takes some time for IV injected cells to be evenly mixed into the systemically circulating blood. Then, it rapidly decreased to below the 10% of the maximum within 2 minutes. With smaller object size threshold, the number of counted objects shows similar kinetics but with significant discrepancies during the first 3 minutes. These discrepancies became very small at later time point as shown in the inset of Fig. 2(b) showing the magnified curve at 15-20 minutes, suggesting that the small-sized cell debris was mostly appeared in the first 3 minutes.

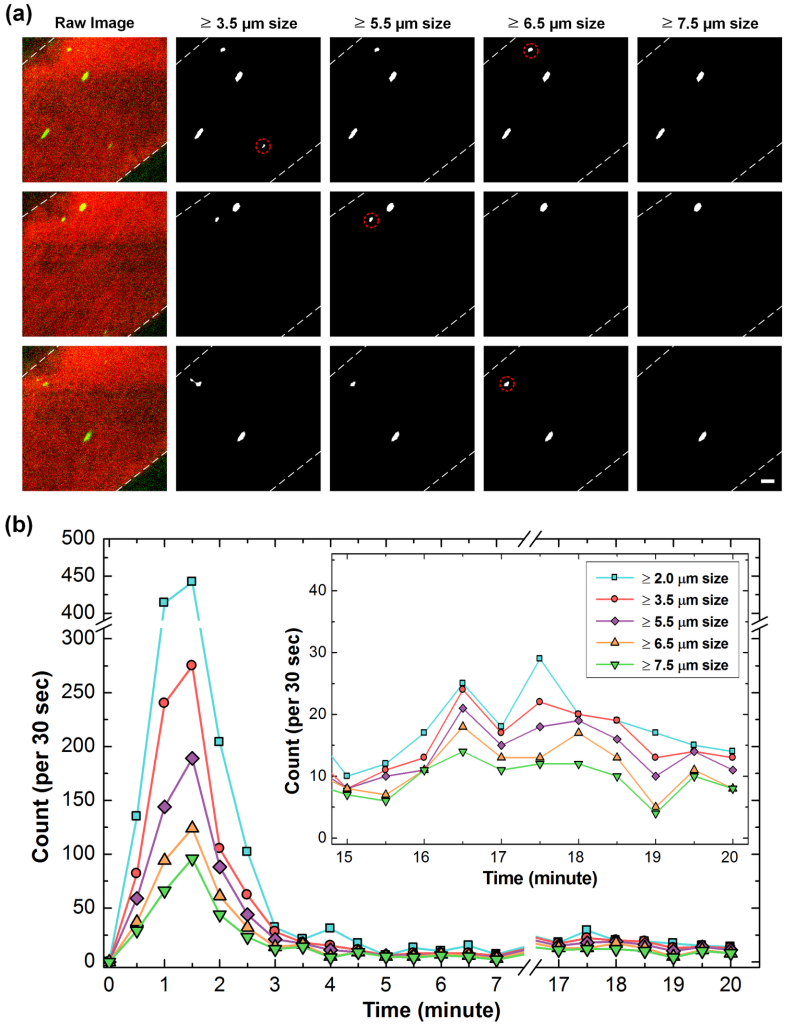

Fig. 2. *In vivo* imaging of intravenous injected circulating CT26 colorectal cancer cells at great saphenous vein (GSV), (a) Raw image and processed results with increasing object size threshold, (b) Time-domain kinetics of the number of detected object with different object size threshold. Inset shows the magnified curve during 15-20 minutes after the IV injection. Scale bar, 20μm.

#235885 - $15.00 USD Received 9 Mar 2015; revised 8 May 2015; accepted 14 May 2015; published 19 May 2015
(C) 2015 OSA

Detailed analysis of collective time-domain kinetics of IV injected CT26 cells and their fragments was performed by size-dependent circulating objects counting. Figure 3(a) shows histograms representing the size distribution of detected circulating objects during 1 minute in different size categories: 2.0-2.5 μm, 2.5-3.5 μm, 3.5-4.5 μm, 4.5-5.0 μm 5.0-5.5 μm, 5.5-6.0 μm, 6.0-6.5 μm, 6.5-7.0 μm, 7.0-7.5 μm and ≥7.5 μm. At 1-2 minutes after the IV injection, the detected number of cellular debris smaller than 2.5 μm or 2.5-3.5 μm range is as many as the intact CT26 cells larger than 7.5 μm. However, after 5 minutes, although the absolute number is dramatically decreased, size category larger than 7.5 μm representing intact circulating CT26 cell became the most frequently detected size category. Figure 3(b) shows the time-dependent changes of detected objects size distribution. At 1-2 minutes, the portion of intact CT26 cells in total detected objects is less than 20%. After 5 minutes, it became almost 50%. Collectively, the rapid disappearance of circulating CT26 cells and the observation of huge number of small cell fragment during the first 3 minutes suggests the massive destruction of IV-injected CT26 cells those were suddenly exposed to extremely harsh environment of blood circulation such as large shear stress, high concentration of serum-protein and cardiac pumping pressure. At 1hour after the IV injection of CT26 cell, the mouse was sacrificed and three major organs of liver, spleen and lung were dissected. Interestingly, very little number of CT26 cells was observed in liver and spleen. On the other hand, numerous CT26 cells and green fluorescent debris were observed in the lung, which suggest that CTC can be easily captured by dense and torturous alveolar capillary network in the lung.

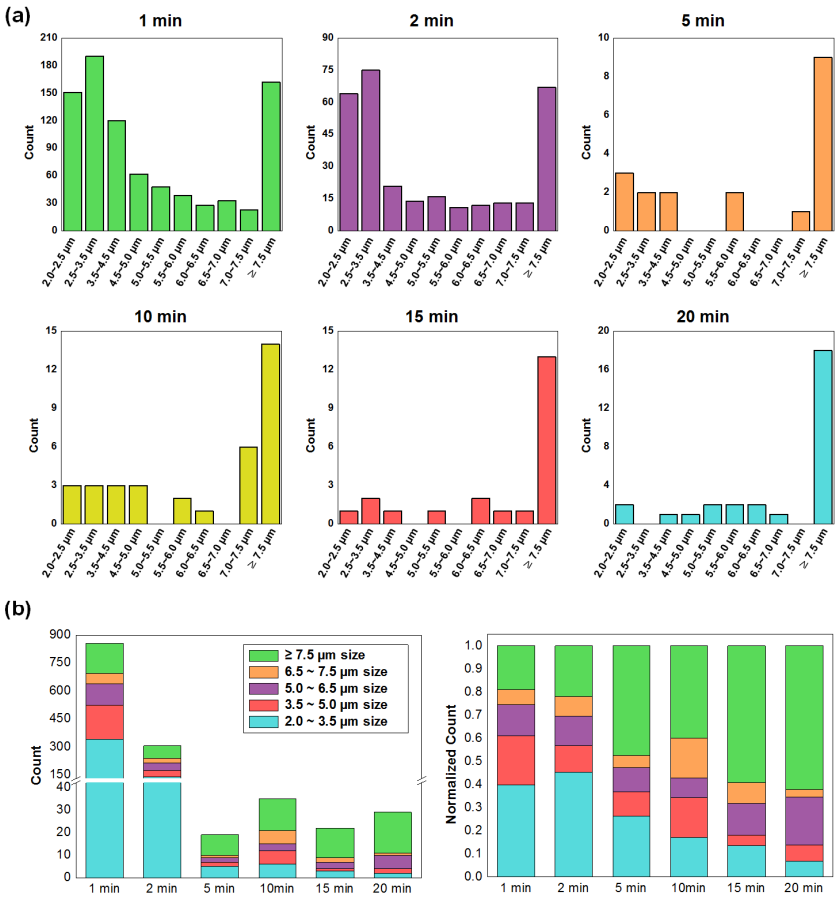

Fig. 3. Size-dependent analysis of circulating tumor cells and cellular fragment detected at GSV, (a) Histogram representing the size distribution of detected circulating objects at different time points, (b) Time-dependent changes of detected objects size distribution.

#235885 - $15.00 USD Received 9 Mar 2015; revised 8 May 2015; accepted 14 May 2015; published 19 May 2015
(C) 2015 OSA

3.2 In vivo quantitation of circulating tumor cells in whole body

As described in section 3.1, the majority of intravenously injected CT26 colorectal cancer cells were quickly disappeared from blood circulation. Only a small fraction of CT26 cells survived and circulated as CTCs. In contrast, when we intravenously injected red blood cells (RBC) labeled by far-red fluorophore DiD, the number of circulating RBC detected at GSV was maintained at similar level over 60 minutes. It suggests that the majority of RBC survived in blood circulation and keep circulating. By utilizing the RBCs as an absolute standard measure that is maintained in whole body circulation, we can estimate the total number of circulating CT26 cells. Figure 4(a) shows the circulating CT26 cells and RBC in GSV captured in video-rate (30 frames/second) by the custom-built confocal microscopy platform. Figure 4(b) shows the time-domain kinetics of circulating CT26 cells and RBCs from the moment right after the intravenous injection for 60 minutes. Each symbol represents the number of detected CT26 cells or 30 seconds. The total number of injected CT26 cells and RBCs was 1 million each. Similar to previous observation, followed by the maximum at 1 minute, the number of circulating CT26 cell was rapidly decreased and then maintained at ~9.7 ± 2.2 per 30 seconds in average over 1 hour.

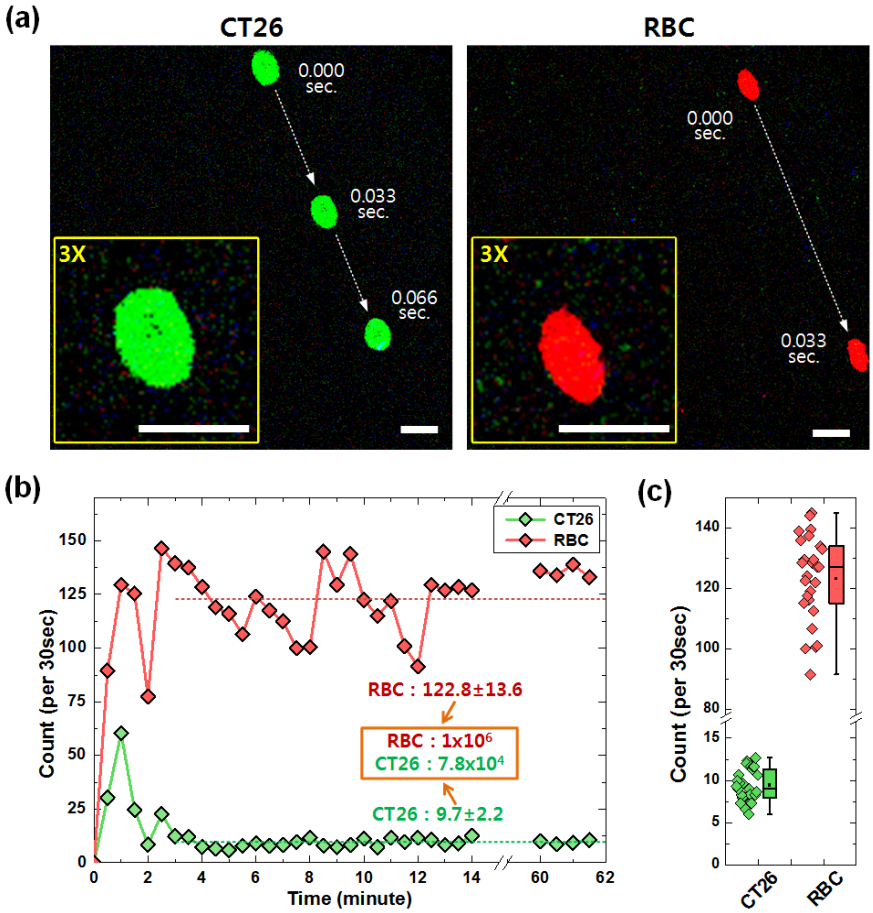

Fig. 4. *In vivo* quantitation of CTCs through hemocytometric analysis of intravenously injected RBCs in whole body, (a) Representative images of fast flowing CT26 cell and RBC captured in GSV at video-rate (30 frames/second). (b) Number of circulating CT26 cells and RBCs detected at GSV after IV injection. After 3 minutes, average account of CT26 cells and RBCs were maintained at ~9.7 ± 2.2 and ~122.8 ± 13.6 per 30 seconds, respectively. (c) Distribution of circulating CT26 cells and RBCs after 3 minutes to 1 hour. Scale bar is 20μm.

#235885 - $15.00 USD Received 9 Mar 2015; revised 8 May 2015; accepted 14 May 2015; published 19 May 2015
(C) 2015 OSA

In contrast, the number of circulating RBC was maintained at initially reached peak value, ~122.8 ± 13.6 per 30 seconds, over 1 hour as shown in Fig. 4(b)-4(c). As the number of total circulating RBCs is presumably 1 million, a relative calibration factor to convert cell count detected for 30 sec to total cell count in blood circulation was calculated to be 8,143. Therefore, the number of total circulating CT26 cells in whole body from 3 minutes after IV injection to 1 hour could be estimated to 78,990.

4. Conclusion

In this study, we implemented a custom-design video-rate confocal microscopy system based on fast-rotating polygonal mirror, which could acquire sub-micron resolution images at 30 frames per second. After the intravenous injection of CT26 colorectal cancer cells and RBCs fluorescently labeled by CFSE and DiD, respectively, we successfully acquired the clear image of individual flowing cells in the great saphenous vein (GSV) in live animal model *in vivo*. With continuous video-rate imaging acquisition, we monitored time-domain kinetics of circulating CT26 cells and RBCs. For reliable counting of intact circulating cells distinguished from cellular debris, we developed an image processing algorithm for the identification of individual objects, calculation of its size and removal of objects smaller than a threshold. The number of circulating CT26 cells detected at GSV rapidly increased right after the injection and reached the maximum at 1.5 minutes. Then it quickly decreased to below the 10% of the maximum within 2 minutes. At the same time, a large number of cellular debris was detected, suggesting massive destruction of CT26 cells due to harsh condition of blood circulation. Interestingly, although more than 90% of injected CT26 cells were destroyed in the first 3 minutes, after the initial dynamic variation, the number of circulating CT26 cells was maintained in similar level over 1 hour, indicating the existence of long-circulating CT26 cells. On the other hand, the number of circulating RBCs was maintained at the initially reached maximum over 1 hour, suggesting that the majority of intravenously injected RBCs could survive in blood circulation. After 3 minutes from the simultaneous intravenous injection of 10^6 CT26 cells and RBCs, the numbers of circulating CT26 cells and RBCs were maintained at ~9.7 ± 2.2 and ~122.8 ± 13.6 per 30 seconds in average over 1 hour. By utilizing the RBCs as an absolute standard measure, the total number of circulating CT26 cells in whole body circulation after the initial massive destruction could be estimated to 78,990, suggesting only ~7.9% of originally injected CT26 cells survived in blood circulation. To note, not only CTCs but also other blood circulating cells could be quantitated by using the newly presented *in vivo* flow cytometric analysis methods, which could be powerful tool for various human disease research using preclinical animal model.

Acknowledgment

This work was supported by the World Class Institute program (WCI 2011-001), the Engineering Research Center program (NRF-2009-0083512), the Global Frontier Project (NRF-M1AXA002-2012M3A6A4054261) of National Research Foundation of Korea and the Converging Research Center Program (2011K000864) funded by the Ministry of Science, ICT and Future Planning, Republic of Korea and the Korea Healthcare Technology R&D Project funded by Ministry of Health and Welfare, Republic of Korea (HN12C0063, HI13C2181).